

# VFISV Inversion Code Documentation for SOLIS/VSM Pipeline Implementation

Brian J. Harker

National Solar Observatory

October 2, 2018

---

Technical Report No. **NSO/NISP-2017-02**

---

## Abstract

Spectral line inversion codes are tools used to interpret spectropolarimetric data; in general, their function is to analyze a set of observed Stokes profiles, and infer the physical properties of the line-formation region in which the Stokes profiles were formed. For the SOLIS/VSM 6302v pipeline, the inversion is based on a Milne-Eddington model atmosphere, optimized to reproduce the observed Stokes profiles of both Fe I lines at 6301.5Å and 6302.5Å. This document provides a detailed overview of the SOLIS/VSM remix of the VFISV (Very Fast Inversion of the Stokes Vector) inversion code, as it is implemented in the SOLIS/VSM pipeline environment.

## Contents

<b>1</b>	<b>The Milne-Eddington Model Atmosphere</b>	<b>2</b>
1.1	Levenberg-Marquardt Inversion . . . . .	5
<b>2</b>	<b>Implementation</b>	<b>6</b>
2.1	Compiling the VFISV Code . . . . .	6
<b>3</b>	<b>Running the VFISV Code</b>	<b>8</b>
3.1	Calling Syntax . . . . .	8
3.1.1	Command Line Arguments . . . . .	8
3.1.2	Examples . . . . .	9
<b>4</b>	<b>Code Functionality</b>	<b>10</b>
4.1	Parameter File . . . . .	10
4.2	Main Program . . . . .	10
4.2.1	Initialization . . . . .	10
4.2.2	Non-magnetic Stokes <i>I</i> Profile Calculation . . . . .	12
4.2.3	Supervisor-Worker Inversion Workflow . . . . .	12
4.3	Inversion Routines . . . . .	14
4.3.1	Reading the Data . . . . .	14
4.3.2	Intensity Thresholding . . . . .	14
4.3.3	Wavelength Calibration . . . . .	16
4.3.4	Parameter Space Boundaries . . . . .	17
4.3.5	Quicklook (QL) Calculation(s) . . . . .	18
4.3.6	Stokes Weights . . . . .	19
4.4	Stokes Profile Synthesis Module . . . . .	20
4.4.1	Levenberg-Marquardt Considerations . . . . .	21
4.4.2	Convergence Strategies/Criteria . . . . .	25
4.4.3	Error Estimation . . . . .	26
<b>5</b>	<b>Output Format</b>	<b>27</b>

## 1 The Milne-Eddington Model Atmosphere

The polarized radiative transfer equations (PRTE) describe attenuation of the Stokes vector,  $\mathbf{I}_\lambda$ , of a beam of polarized light as it propagates, in the direction  $s$ , through some medium. Formally, it is given here as

$$\mu \frac{d\mathbf{I}_\lambda}{ds} = \mathbf{K}_\lambda (\mathbf{I}_\lambda - \mathbf{S}_\lambda), \quad (1)$$

where  $\mu$  is the cosine of the heliocentric angle, and  $\mathbf{K}_\lambda$  and  $\mathbf{S}_\lambda$  are the propagation matrix and source function vector, respectively. Note that, throughout this document, a  $\lambda$ -subscript denotes a wavelength-dependent quantity (though it may be dropped for notational clarity).

If we model both continuum and line absorption processes, then

$$\mathbf{K}_\lambda = \mathbf{1} + \eta_0 \mathbf{\Phi}_\lambda = \begin{bmatrix} \eta_I & \eta_Q & \eta_U & \eta_V \\ \eta_Q & \eta_I & \rho_V & -\rho_U \\ \eta_U & -\rho_V & \eta_I & \rho_Q \\ \eta_V & \rho_U & -\rho_Q & \eta_I \end{bmatrix}_\lambda \quad (2)$$

where  $\mathbf{1}$  is a  $4 \times 4$  identity matrix,  $\eta_0$  is the ratio of line-to-continuum absorption coefficients, and the matrix  $\mathbf{\Phi}_\lambda$  includes both absorption and magneto-optical effects, parameterized by the magnetic and thermodynamic properties of the model atmosphere under the classical Zeeman effect regime. Expressions for these matrix elements may be found in Landi Degl'Innocenti and Landolfi (2004) and references therein. They are reproduced here for completeness, with the wavelength dependence implied but dropped from the notation for clarity.

$$\eta_I = 1 + \frac{1}{2}\eta_0 \left[ \phi_\pi \sin^2 \gamma + \frac{1}{2} (\phi_{\sigma_r} + \phi_{\sigma_b}) (1 + \cos^2 \gamma) \right] \quad (3)$$

$$\eta_Q = \frac{1}{2}\eta_0 \left[ \phi_\pi - \frac{1}{2} (\phi_{\sigma_b} + \phi_{\sigma_r}) \right] \sin^2 \gamma \cos 2\chi \quad (4)$$

$$\eta_U = \frac{1}{2}\eta_0 \left[ \phi_\pi - \frac{1}{2} (\phi_{\sigma_b} + \phi_{\sigma_r}) \right] \sin^2 \gamma \sin 2\chi \quad (5)$$

$$\eta_V = -\frac{1}{2}\eta_0 (\phi_{\sigma_r} - \phi_{\sigma_b}) \cos \gamma \quad (6)$$

$$\rho_Q = \frac{1}{2}\eta_0 \left[ \psi_\pi - \frac{1}{2} (\psi_{\sigma_b} + \psi_{\sigma_r}) \right] \sin^2 \gamma \cos 2\chi \quad (7)$$

$$\rho_U = \frac{1}{2}\eta_0 \left[ \psi_\pi - \frac{1}{2} (\psi_{\sigma_b} + \psi_{\sigma_r}) \right] \sin^2 \gamma \sin 2\chi \quad (8)$$

$$\rho_V = -\frac{1}{2}\eta_0 (\psi_{\sigma_r} - \psi_{\sigma_b}) \cos \gamma \quad (9)$$

The  $\phi$  and  $\psi$  terms are the absorption and anomalous dispersion profiles (and are functions of wavelength) for the  $\pi$ ,  $\sigma_r$ , and  $\sigma_b$  Zeeman components involved in the transition which gives rise to the absorption line itself. As can be seen above, the matrix elements themselves depend on the vector magnetic field explicitly through the inclination,  $\gamma$ , and azimuthal angle,  $\chi$ , and also have a dependence on the field strength through the Voigt and Faraday-Voigt spectral line shapes, given by:

$$H_\lambda(a_{\text{dc}}, v) = \frac{a_{\text{dc}}}{\pi} \int_{-\infty}^{+\infty} \frac{e^{-t^2}}{a_{\text{dc}}^2 + (v-t)^2} dt \quad (10)$$

$$F_\lambda(a_{\text{dc}}, v) = \frac{1}{\pi} \int_{-\infty}^{+\infty} \frac{(v-t)e^{-t^2}}{a_{\text{dc}}^2 + (v-t)^2} dt \quad (11)$$

$$v = \frac{\lambda - \lambda_0(1 + v_{\text{los}}/c) \pm \Delta\lambda_Z}{\Delta\lambda_D}, \quad (12)$$

where  $\lambda_0$  is the line-center wavelength,  $v_{\text{los}}$  is the relative line-of-sight (LOS) velocity between source and observer,  $a_{\text{dc}}$  is the atomic damping constant of the line,  $\Delta\lambda_D$  is the Doppler line-width, and  $\Delta\lambda_Z$  is the Zeeman splitting of the line (which is itself a function of the atomic energy levels of the transition as well as magnetic field strength,  $B$ ). The absorption ( $\phi$ ) and anomalous dispersion profiles ( $\psi$ ) are then calculated as:

$$\phi_i = \sum_{j=1}^{N_z} S_j^{(i)} H_\lambda(a_{\text{dc}}, v_j) \quad (13)$$

$$\psi_i = \sum_{j=1}^{N_z} S_j^{(i)} F_\lambda(a_{\text{dc}}, v_j), \quad (14)$$

where  $i = \{\pi, \sigma_r, \sigma_b\}$ ,  $N_z$  is the number of Zeeman subcomponents of the  $i^{\text{th}}$  component, and  $S_j^{(i)}$  is the Zeeman strength of the  $j^{\text{th}}$  Zeeman subcomponent. The strengths are functions of the quantum numbers of the upper and lower energy levels of the Zeeman subcomponents involved in the transition. Analytical expressions for  $S_j^{(i)}$  are given in Table 3.1 of Landi Degl'Innocenti and Landolfi (2004) for all allowed transitions. For a normal Zeeman triplet (like the Fe I 6302.5Å line), there is only one  $\pi$ ,  $\sigma_r$ , and  $\sigma_b$  Zeeman component, so  $S_j^{(i)} = 1 \forall i, j$ . However, for an anomalous Zeeman triplet (like the Fe I 6301.5Å line), there are multiple Zeeman subcomponents, such that we require:

$$\sum_{j=1}^{N_z} S_j^{(i)} = 1, \forall i. \quad (15)$$

The source function vector ( $\mathbf{S}_\lambda$  in Equation (1)) describes the ratio of emission to absorption in the beam, and includes both continuum and line contributions, so that

$$\mathbf{S}_\lambda = S_c \hat{\mathbf{e}} + \eta_0 S_l \Phi_\lambda \hat{\mathbf{e}}, \quad (16)$$

where  $\hat{\mathbf{e}} = (1, 0, 0, 0)^T$ ,  $S_c$  is the continuum source function, and  $S_l$  is the line source function. Assuming local thermodynamic equilibrium reduces both the continuum and line source functions to the Planck function at the local temperature,  $B_\lambda(T)$ . Adopting a Milne-Eddington (ME) relation for the source function variation as a linear function of optical depth,

$$S_c = S_l = B_\lambda(T) = S_0 + S_1 \tau = S_0(1 + \beta_0 \tau), \quad (17)$$

the PRTE admits an analytical solution for the model Stokes profiles,  $\mathbf{I}_\lambda^M$ , given here as

$$\frac{\mathbf{I}_\lambda^M}{I_c} = \left[ (1 - \beta) \mathbf{1} + \beta (\mathbf{1} + \eta_0 \Phi_\lambda)^{-1} \right] \hat{\mathbf{e}} \quad (18)$$

$$\beta = \frac{\mu \beta_0}{1 + \mu \beta_0}. \quad (19)$$

Note that  $\beta_0 = S_1/S_0$  represents the inverse of the characteristic length scale over which the source function changes appreciably, and  $I_c$  denotes the observed local continuum intensity. Note also that the Eddington-Barbier approximation states that the emergent continuum intensity at a position  $\mu$  on the solar disc is given by  $S_c(\tau = \mu)$ , so that we have the relation  $I_c = S_0 + \mu S_1$ , coupling the (observed) continuum intensity with the source function coefficients. The source function coefficients *must* obey this constraint at all points in the inversion.

At a modest 1 arcsec spatial sampling, SOLIS/VSM does not fully resolve magnetic structures. Therefore, we introduce a geometrical factor which represents the fraction of the pixel occupied by magnetic field, and as such, must be in the range  $[0, 1]$ . This is the magnetic filling-factor,  $\alpha$ , and is a zeroth-order attempt at accounting for limited spatial resolution, by allowing the pixel to contain a mixture of Stokes profiles from both magnetic and non-magnetic atmospheres coexisting within the same pixel. The Stokes vector then becomes a linear superposition of the magnetic and non-magnetic profiles, weighted by  $\alpha$ ,

$$\mathbf{I}_\lambda^M \leftarrow \alpha \mathbf{I}_\lambda^M + (1 - \alpha) I_\lambda^{\text{nm}} \hat{\mathbf{e}}. \quad (20)$$

The non-magnetic profile,  $I_\lambda^{\text{nm}}$ , is synthesized from the same model parameter vector as the magnetic profile, but magnetic field strength is set to zero. This is preferable to using (e.g.) an average observed quiet-sun profile constructed from low-polarization Stokes  $I$  profiles in the surroundings, since we would have to deconvolve the instrumental profile from the average quiet-sun profile before mixing it with the magnetic profile, and then re-convolve with the instrumental profile. We like to avoid deconvolution at all costs, thank you very much. To account for the smearing effects of the SOLIS/VSM instrumental profile, the synthetic Stokes vector  $\mathbf{I}_\lambda^M$  is convolved with a Gaussian kernel with a half-width at half-maximum (HWHM) of 22.5mÅ. This is equivalent to considering a macroturbulent velocity,  $v_{\text{mac}}$ , of  $1.3081 \times 10^5$  cm/sec, which is held constant during the inversion.

As shown above, the Milne-Eddington (ME) atmosphere is characterized by the following assumptions: 1) the line-formation region is under local thermodynamic equilibrium, 2) the source function varies linearly with optical depth, 3) all other physical properties are constant over the line-formation region, and 4) the polarized radiative transfer is described by the classical Zeeman effect. As such, it is a simple (but widely-used) model. Since we do not consider gradients with respect to optical depth of any parameter except the source function, the ME atmosphere represents a kind of average of the true parameters over the height of line-formation. Under these assumptions, the PRTE admits an analytical solution, known as the Unno-Rachkovsky solutions (Unno, 1956; Rachkovsky, 1962, 1963, 1967), which are functions parameterized by the free model parameter vector,  $\mathbf{p} = [B, \gamma, \chi, v_{\text{los}}, \Delta\lambda_D, a_{\text{dc}}, \eta_0, S_0, \mu S_1, \alpha]$ . The model parameters are listed and summarized below for clarity:

- $B$ : Magnetic field strength
- $\gamma$ : Inclination of the magnetic field vector relative to the LOS

- $\chi$ : Azimuthal angle of the transverse component of the magnetic field vector
- $v_{\text{los}}$ : Relative LOS velocity between source and observer
- $\Delta\lambda_D$ : Doppler line width
- $a_{\text{dc}}$ : Atomic damping constant of the line
- $\eta_0$ : Line-to-continuum opacity ratio
- $S_0$ : Source function continuum
- $\mu S_1$ : heliocentric  $\mu \times$  Source function gradient
- $\alpha$ : Magnetic filling-factor
- $v_{\text{mac}}$ : Macroturbulent velocity

### 1.1 Levenberg-Marquardt Inversion

The VFISV (Very Fast Inversion of the Stokes Vector) inversion code executes a general non-linear least-squares optimization of a Milne-Eddington model atmosphere to reproduce Stokes profiles which best fit the actual observations. It has been tuned for speed to enable the SOLIS/VSM 6302v pipeline to invert *every* pixel on the solar disc in a short time ( $\sim 10$  minutes).

The function to be minimized by the inversion algorithm is the following  $\chi^2$ -like merit function, which quantifies the agreement between the Stokes vector ( $\mathbf{I}^M$ ) synthesized in the model atmosphere (parameterized by  $\mathbf{p}$ ) and the observations ( $\mathbf{I}^O$ ), given here explicitly as

$$\chi^2(\mathbf{p}) = \frac{1}{\nu} \sum_i \sum_{j=1}^{N_\lambda} w_{ij}^2 [\mathbf{I}_i^O(\lambda_j) - \mathbf{I}_i^M(\lambda_j; \mathbf{p})]^2, \quad (21)$$

where  $i = I, Q, U, V$ . The number of degrees of freedom in the optimization is given by  $\nu$ , and  $N_\lambda$  is the number of observed wavelengths spanning the bandpass containing the lines to be inverted. The quantities  $w_{ij}$  are weighting factors (entering quadratically), traditionally used to adjust the contribution of different wavelengths to the total deviation between the modelled and observed spectral line, and are discussed further in Section 4.3.6.

Given an initial guess for the model parameters, the inversion code uses a Levenberg-Marquardt non-linear least squares optimization algorithm to perform the inversion. At each step, perturbations to the current ME model parameters are calculated, and the new set of model parameters are used to synthesize Stokes profiles. The  $\chi^2$  merit function is calculated via Equation (21) and tested against the current value. If an improvement (reduction) is found, the perturbations are accepted and the model parameters are updated for the next iteration. If not, new perturbations are calculated. This iterative improvement proceeds until one or more convergence criteria are satisfied (more on this in Section 4.4.2), at which time the algorithm outputs the current model parameters as the solution to the inversion problem; i.e., the physical parameters of the ME model atmosphere in which the observed Stokes profiles were formed.

## 2 Implementation

The VFISV code used in the SOLIS/VSM 6302v production pipeline is meant to handle standard SOLIS/VSM Level-0.5 spectra contained in FITS files. For full-disc observations, this consists of 2048 fully-calibrated (dark-corrected, flat-fielded, polarization-calibrated) scanlines, each containing 128 wavelength samples for 4 Stokes profiles for 2048 spatial pixels along the spectrograph slit. This Section focuses on various issues related to the implementation of the code (libraries, compilation) in the 6302v pipeline environment.

### 2.1 Compiling the VFISV Code

This Section contains a short list of implementation details relating to what is required to compile the VFISV code.

- Language: Fortran 90 (with a single utility function written in C).
- Architecture: Developed for 64-bit machines.
- MPI parallelization: VFISV depends on the Message Passing Interface (MPI) for parallel processing of individual scanlines. The MPI interface is provided by MPICH-2, the MPI implementation from Argonne National Laboratory. MPICH-2 is a high performance and widely portable implementation of the MPI standard.
- Compiler: On the machine used for development of the code, MPICH-2 for Fortran was built using the Intel `ifort` compiler. As such, the MPI wrapper compiler `mpif90` has a backend based on `ifort`. No (serious) attempt was made at compiling/running the code with any other compiler. Fair warning. The single utility function written in C is compiled with the GNU `gcc` compiler.
- Compiler Flags/Optimizations:
  - `-fast` : Maximizes speed across the entire program. On Itanium(R)-based systems, this option sets options `-ipo`, `-O3`, and `-static`. On IA-32 and Intel(R) EM64T systems, this option sets options `-ipo`, `-O3`, `-no-prec-div`, `-static`, and `-xP`. Note that programs compiled with the `-xP` option will detect non-compatible processors and generate an error message during execution. This optimization has a dramatic impact on runtime; the code was tested without this optimization flag, and the results were identical to those obtained with this optimization, although they were obtained *much* slower.
  - `-prec-div` : Improves precision of floating-point divides; it has some speed impact. With some optimizations, such as `-xN` and `-xB`, the compiler may change floating-point division computations into multiplication by the reciprocal of the denominator. For example,  $A/B$  is computed as  $A * (1/B)$  to improve the speed of the computation. However, sometimes the value produced by this transformation is not as accurate as full IEEE division. When it is important to have fully precise IEEE division, use `-prec-div` to disable the floating-point division-to-multiplication optimization. The result is more accurate, with some loss of performance.
  - `-check all` : Enables all `-check` options. NOTE: while not routinely compiled with this flag, it can be helpful to occasionally check for certain conditions at runtime (i.e. after major changes to the code), like out-of-bounds array subscripts.

- `-warn all` : Enables all diagnostic warning messages. NOTE: while not routinely compiled with this flag, it can be helpful to occasionally check for certain conditions at compile time (i.e. after major changes to the code), like unused variables, etc.
  - `-g` : Enables debugging support. Not routinely compiled with this flag.
  - `-p` : Enables `gprof` profiling support. Not routinely compiled with this flag.
- Required libraries: MPI, LAPACK, CFITSIO
- Makefile: The Makefile included with the code is sufficiently general that it should work for most machines/environments, provided the right paths are set. To run in other environments, one just needs to make sure that the required libraries (MPI, LAPACK, CFITSIO) are installed, and the path(s) to these libraries are correctly specified.
- To compile the code, simply run `make vfishv`.
  - To install the `vfisv.x` executable into the SOLIS `bin` directory on a production/reprocessing machine, simply run `make install`. Note that this strips the “.x” file extension to produce the `vfisv` binary executable in the `bin` directory.
  - To remove all compiled files, modules, objects (etc.), simply run `make clean`.
  - To create a dated tarball of the VFISV codebase and support files (IDL functions, e.g.), simply run `make backup`.



## 3 Running the VFISV Code

This Section contains information detailing how to run the VFISV code. Specifically, I present here summaries of the calling syntax, with appropriate command line arguments, and give examples of how to run the code in various modes.

### 3.1 Calling Syntax

The default syntax for running the VFISV inversion code is as follows (note that square brackets denote optional arguments):

```
$ mpirun -np NP /home/solis/bin/vfisv [-v] [-vv] [-P] -i /path/to/Level-0.5/dir  
-w /path/to/Level-1/output/tmp/dir [-s s1 [s2]] [-p p1 [p2]]
```

where `NP` is the number of MPI processes requested for the inversion. Note that the supervisor MPI rank does no work inverting scanlines itself, so only `NP-1` scanlines can be inverted simultaneously (see Section 4.2.3).

#### 3.1.1 Command Line Arguments

- `-i` : [REQUIRED] Specify the path to the directory containing SOLIS/VSM Level-0.5 scanline FITS files.
- `-w` : [REQUIRED] Specify the path to the directory which will contain SOLIS/VSM Level-1 FITS file output from the inversion. This directory will be created if it does not already exist.
- `-s` : [OPTIONAL] Specify a range of scanlines to invert. This is useful for inverting only a fraction of a full-disc observation, or for inverting entire area-scan observations. If only a single scanline index is provided (`-s s1`), the code will invert only that scanline; if two indices are provided (`-s s1 s2`), the code will invert all scanlines between `s1` and `s2`, inclusive.
- `-p` : [OPTIONAL] Specify a range of pixels to invert. This is useful (in combination with `-s`) for inverting only a rectangular subset of the available dataset (e.g., if you're interested in a particular active region). If only a single pixel index is provided (`-p p1`), the code will invert only that pixel; if two indices are provided (`-p p1 p2`), the code will invert all pixels between `p1` and `p2`, inclusive.
- `-v` : [OPTIONAL] Switch on verbose messages (for debugging). NOTE: this will produce *a lot* of screen output, so it is not suitable for regular full-disc inversions, but rather intended to be used on a single-pixel basis for development and/or diagnosing potential issues.
- `-vv` : [OPTIONAL] Switch on extra verbose messages (for debugging). This produces much more screen output than the `-v` option. `-vv` implies `-v`.
- `-P` : [OPTIONAL] Switch on "preview mode", which rapidly generates a Level-1 quicklook file from non-defringed Level-0.5 spectra. This is *only* used by the observers to quickly get feedback on instrument pointing, (e.g.) during area-scans.

### 3.1.2 Examples

A full-disc 6302v observation was taken on 08 July 2015. To invert the Level-0.5 spectra for this observation (contained in the directory `k4v9s150708t175025_oid114363777241750_cleaned`) using 16 MPI processes, and place the resulting Level-1 file(s) in the appropriate tmp directory, run:

```
$ mpirun -np 16 /home/solis/bin/vfisv -i
/path/to/v9s/201507/k4v9s150708/k4v9s150708t175025_oid114363777241750_cleaned
-w /path/to/vsm/tmp/k4v91150708t175025
```

To invert only those scanlines between 512 and 1536 (inclusive), run:

```
$ mpirun -np 16 /home/solis/bin/vfisv -i
/path/to/v9s/201507/k4v9s150708/k4v9s150708t175025_oid114363777241750_cleaned
-w /path/to/vsm/tmp/k4v91150708t175025 -s 512 1536
```

To invert only those scanlines between 512 and 1536, and only in Camera A (e.g.), run:

```
$ mpirun -np 16 /home/solis/bin/vfisv -i
/path/to/v9s/201507/k4v9s150708/k4v9s150708t175025_oid114363777241750_cleaned
-w /path/to/vsm/tmp/k4v91150708t175025 -s 512 1536 -p 1 1024
```

To invert only those scanlines between 512 and 1536, and only in Camera B (e.g.), run:

```
$ mpirun -np 16 /home/solis/bin/vfisv -i
/path/to/v9s/201507/k4v9s150708/k4v9s150708t175025_oid114363777241750_cleaned
-w /path/to/vsm/tmp/k4v91150708t175025 -s 512 1536 -p 1024 2048
```

To invert only a single pixel with verbose messages for debugging, run:

```
$ mpirun -np 2 /home/solis/bin/vfisv -i
/path/to/v9s/201507/k4v9s150708/k4v9s150708t175025_oid114363777241750_cleaned
-w /path/to/vsm/tmp/k4v91150708t175025 -s 512 -p 768 -v
```

NOTE: for single-pixel inversion, you *must* use `mpirun -np 2`, or you will get an error message complaining that too many MPI processes would be used:

```
$ [ERROR] MPI_NUM_RANKS > Number of scanlines to invert!"
$ [ERROR] Check your mpirun command line..."
```

In general, you must use an appropriate number of MPI ranks for the inversion; if the number of MPI ranks is undersubscribed relative to the number of scanlines to invert, at least one MPI worker rank will never receive a scanline index assignment it is waiting for, and the code will *never* successfully exit. Since that MPI worker rank will perpetually wait for an assignment that will never come, it will never be available to receive the termination message from the MPI supervisor rank, and will hang the program execution. Hence, this warning message and exit condition are needed just to be safe.

## 4 Code Functionality

### 4.1 Parameter File

The file `params.f90` contains constant parameters and global variable declarations used throughout the VFISV code. Any module requiring access to a parameter or global variable must include the line `USE PARAMS` in the module header. For example, the parameter file contains declarations for the following quantities (among many others):

- Fortran 90 variable kind types and numerical constants, e.g.:  
`INTEGER, PARAMETER :: DP = KIND(1.0D0)`
- Physical constants, e.g.:  
`REAL(DP), PARAMETER :: DPI = 3.141592653589793238462643_DP`
- Runtime constants, e.g.:  
`INTEGER, PARAMETER :: NUM_SCANS = 2048`
- Input/output configuration, e.g.:  
`INTEGER, PARAMETER :: NUM_LEV1_MEMAPS = 12`
- Quicklook and inversion engine parameters, e.g.:  
`INTEGER, PARAMETER :: MAX_ITERS = 100`
- Line-formation & spectral parameters, e.g.:  
`REAL(DP), PARAMETER :: LAB_LAMBDA0 = 6302.4995_DP`
- Global variables that are initialized at runtime, e.g.:  
`CHARACTER(LEN=256), DIMENSION(NUM_SCANS) :: OBSFILES`

### 4.2 Main Program

The main VFISV program is nothing more than an initialization, bookkeeping, and collection routine which dispatches scanline inversion assignments to MPI worker ranks and collects/assembles the results received back from the MPI worker ranks. There are three main tasks coordinated by the main VFISV program: initialization, non-magnetic Stokes *I* profile calculation, and supervisor-worker inversion workflow, which are detailed in the following subsections.

#### 4.2.1 Initialization

The first step in the program is to perform sanity checks on command line input.

##### SANITY CHECK #1:

The given Level-0.5 obs directory (`INDIR`) and Level-1 output directory (`WORKDIR`) are tested for existence. If `INDIR` is not present on the command line or does not exist, VFISV exits with an error. If `WORKDIR` is not present on the command line, VFISV exits with an error. However, if it is present on the command line, but does not exist in the filesystem, a system call will create it. Note that the test for existence relies on the `INQUIRE` function, used with the `ifort` extension argument `DIRECTORY` to set the boolean flag `DIR_EXISTS`:

```
INQUIRE ( DIRECTORY=INDIR, EXIST=DIR_EXISTS ).
```

The use of this extension makes the VFISV code system-dependent and non-portable. Once `INDIR` is validated, the directory is probed to determine the spatial size of the dataset it contains. The subroutine `DATA_INIT()` is called, which determines the number of files matching the "`k?v9s*`" regular expression and sets the global variable `NUM_FILES` equal to this number. One of the Level-0.5 FITS files contained in this directory is then opened and used to determine the number of spatial pixels along the scanline, `NUM_PIX`. The various arrays which are dependent on the spatial dimensionality of the dataset are then dynamically allocated. This allows the inversion code to handle datasets of arbitrary spatial dimensionality, so that the code is not limited to inversions of 2048 scanlines, each containing Stokes spectra for 2048 pixels. In the SOLIS/VSM production pipeline, `INDIR` typically points to a directory containing defringed spectra in an obs' tmpdir, for example:

```
/path/to/vsm/tmp/k?v90YYMDDtHHMMSS/k?v9sYYMDDtHHMMSS_oidXXXXXXXXXXXXHHMM_cleaned.
```

However, when running in "preview mode", `INDIR` will point instead to the directory containing the non-defringed spectra, for example:

```
/path/to/vsm/tmp/k?v90YYMDDtHHMMSS/oidXXXXXXXXXXXXHHMM,
```

and some special manipulation is used to properly set the value of `OBSID` for the `DATA_INIT()` subroutine.

#### **SANITY CHECK #2:**

If provided on the command line, `SCAN_START` and `SCAN_END` are checked to ensure they are both positive and less than the maximum number of scanlines/pixels (typically 2048), determined from `DATA_INIT()`. If not present, VFISV defaults to a full-disc inversion.

Once the command line input has been validated, runtime properties of the inversion code can be initialized:

#### **CAMERA TYPE INITIALIZATION:**

The year of the observation is extracted from `INDIR`. The value of the `CAMTYPE` variable is set to `ROCKWELL` for pre-2010 observations, or to `SARNOFF` for observations from 2010 to present. This variable allows for easy discrimination in the code between the two camera eras, and is required for the following:

- Discrimination between on-disc and sky pixels, which uses a different intensity threshold for each camera era. The on-disc intensity threshold for the Rockwell camera (2003-2009) is set at 1500 counts, while for the Sarnoff camera (2010-present) the threshold is 5000 counts.
- The continuum window (range of wavelengths for which the continuum intensity is calculated) is different for the two cameras, due to the different illuminated portions of the camera CCDs. The same is true for the individual line windows (range of wavelengths which approximately centrally-bracket both the solar and telluric lines).

NOTE: any other camera-specific quantities can be set within the same routine that performs the above initializations (`SET_CAMTYPE_PROPERTIES()`).

**DATA FILE INITIALIZATION:**

Once the input and output directories have been validated, the subroutine `FILE_INIT()` inspects the contents of the `INDIR` directory, and looks for standard SOLIS/VSM 6302v Level-0.5 FITS files, again using `INQUIRE` to test for existence. For bookkeeping purposes, *all* FITS files in the input directory are listed in the `OBSFILES(:)` array, but only those which are to be inverted (which have an index between `SCAN_START` and `SCAN_END`) are listed in the `INVFILES(:)` array. This is for proper handling of cases where only a subset of the observed scanlines are being inverted, as well as for handling inversions of true area-scan observations.

**ME MODEL INITIALIZATION:**

Model parameters which are considered free parameters of the fit are marked as such in the `FREE(:)` array, which is a boolean array with `.TRUE.` entries for free parameters and `.FALSE.` entries for fixed parameters. This allows the user to invert for any combination of free and fixed parameters, and the algorithm will automatically scale the sizes of its working spaces accordingly. In the current implementation, only  $\alpha$  and  $v_{\text{mac}}$  are considered fixed parameters, set to a respective constant value for the entire run of the inversion (see Section 4.3.5). In addition, if any regularization of the free model parameters is required, this can be specified in the same manner, by setting the corresponding entry of the `REGUL_FLAG(:)` array to `.TRUE.`, and specifying the functional form of the regularization in the subroutine `REGULARIZE()`.

**4.2.2 Non-magnetic Stokes  $I$  Profile Calculation**

The non-magnetic Stokes  $I$  profile used in the inversion is calculated as an average Stokes  $I$  profile over a local neighborhood around each pixel. A  $25 \times 25$  pixel<sup>2</sup> neighborhood is used, centered on each pixel. Only pixels with polarization degree,  $p$ , given by:

$$p = \frac{\text{maxval} \left( \sqrt{Q_\lambda^2 + U_\lambda^2 + V_\lambda^2} \right)}{I_c} \quad (22)$$

less than  $10^{-2}$  are allowed to contribute to the neighborhood average. There can be situations where no neighborhood pixels satisfy this criterion, for example in the deep umbra of larger sunspots. In this situation, there would be no non-magnetic Stokes  $I$  profile available for these pixels. Simply increasing the size of the window so that (say) the largest anticipated magnetic structure still has some neighboring quiet-Sun pixels is computationally inefficient and leads to prohibitively long runtimes. To alleviate this problem, a simple linear interpolation between neighboring profiles is used to fill in these gaps. Note that the non-magnetic Stokes vector is assumed to be unpolarized, i.e., there is no non-magnetic Stokes  $Q$ ,  $U$ , or  $V$  signal. The non-magnetic profile is used in several support roles prior to the actual inversion itself, in which the non-magnetic profile is synthesized from the same model parameters as the magnetic profile (but with no magnetic field; see Section 4.4).

**4.2.3 Supervisor-Worker Inversion Workflow**

The MPI supervisor rank (`MPI_RANK=0`) is responsible for coordinating the workflow amongst the other MPI worker ranks, which are themselves responsible for performing the actual inversion of the Stokes profiles in each SOLIS/VSM Level-0.5 scanline. To facilitate this coordination, the MPI supervisor rank must be aware of which MPI worker rank is inverting which scanline, and where the results should be placed in the resulting output array(s). The MPI supervisor rank does this by dispatching the scan index of a scanline to be inverted to each MPI worker

rank, and receiving the inverted parameters back from that worker rank, as shown schematically in Figure 1. When receiving results from an MPI worker rank (using the `MPI_RECV()` subroutine), an array of supplementary information is also passed back via the `MPI_STAT(:)` argument. `MPI_STAT(MPI_STATUS_SIZE)` is an array of integers containing the source rank, tag, and error code of the received message. `MPI_SOURCE`, `MPI_TAG`, and `MPI_ERROR` are the indices of the entries for the source rank, tag, and error codes of the received message. By setting these values, each MPI worker rank can effectively communicate back to the MPI supervisor rank where the results should be placed in the output array, as well as indicating that it is immediately available to invert another scanline. On average, this speeds up the algorithm by about 15% over a sequentially-ordered dispatch-and-return scheme. The following outline details how the MPI supervisor rank coordinates the workflow of the MPI worker ranks until the entire dataset has been inverted:

- The MPI supervisor rank dispatches the initial batch of scanline indices to worker ranks.
- Each MPI worker rank receives a scanline index, calculates the non-magnetic Stokes  $I$  profiles for that scanline, and performs the ME inversion on the Stokes profiles in that scanline.
- Each MPI worker rank dispatches the ME results back to the MPI supervisor rank, setting `MPI_STAT(MPI_TAG)` equal to the scanline index it initially received from the MPI supervisor rank.
- The MPI supervisor rank is always listening, and accepts results from any MPI worker rank, and uses the MPI tag located in `MPI_STAT(MPI_TAG)` to place the received results in the correct place in what will eventually be the output data product array written to an external FITS file.
- The MPI rank of the sender is identified by the value of `MPI_STAT(MPI_SOURCE)`, so that the MPI supervisor rank knows which MPI worker rank it has just received results from, and can dispatch another scanline index to that MPI rank.
- The MPI supervisor rank then dispatches the next available scanline index to that same MPI worker rank. The cumulative number of scanline indices sent is updated.
- This process repeats until results from all invertible scanlines have been received, and the total number of scanline indices dispatched (and number of resulting arrays received) by the MPI supervisor rank is equal to the number of scanlines to be inverted (`NUM_SCANS`). The MPI supervisor rank then sends a special termination message to all MPI worker ranks to indicate there is no more work to be done, so that each MPI worker rank exits the loop in which it expects to receive a scanline index from the MPI supervisor rank.
- Note: all MPI subroutine calls are followed by a sanity check on the error flag, `IERR`, set by the previously-called MPI subroutine. This ensures correct operation and allows the inversion code to exit gracefully should anything go wrong with a call to an MPI subroutine.

The MPI supervisor rank rearranges the received output into an array that follows SOLIS/VSM 6302v Level-1 standards, then writes it to an external FITS file with a minimal header (which will later be populated downstream in the Level-1 to Level-2 processing). More detail on the output format is given in Section 5. Runtime and inversion statistics are calculated and reported by the MPI supervisor rank, then all MPI ranks synchronize and exit. At this point, the VFISV inversion is complete.

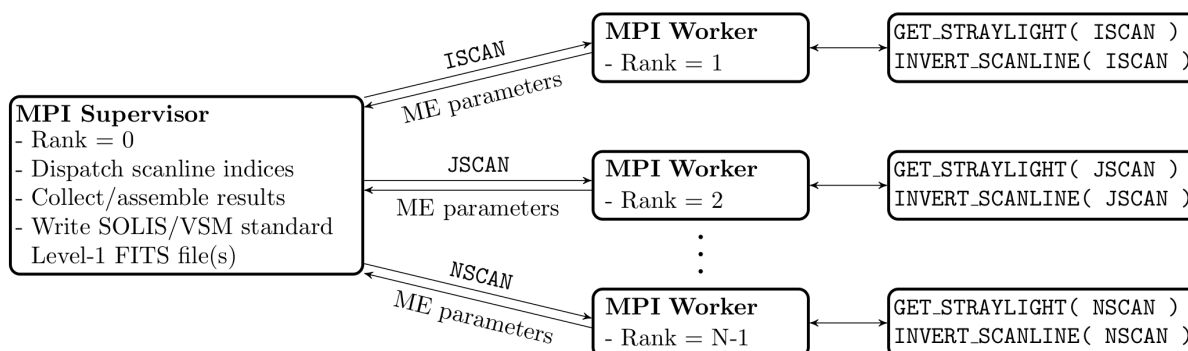


Figure 1: Schematic flowchart describing division of labor amongst MPI ranks.

### 4.3 Inversion Routines

This Section outlines the main subroutines used in the actual inversion subroutine, `INVERT_SCANLINE()`. For reference, Figure 2 shows a schematic flowchart of the major steps involved in the inversion of a SOLIS/VSM 6302v Level-0.5 scanline. Each major block in the flowchart is the subject of a subsection below.

#### 4.3.1 Reading the Data

VFISV relies on the CFITSIO library (and the FORTRAN extensions therein) for reading and writing FITS files. Once an MPI worker rank receives the scanline index for an inversion, the first step is to read that scanline data file. A free logical unit number is retrieved and associated with the file. The file is opened, and the image dimensions are read from the FITS header (via the `NAXIS` keywords). A buffer of suitable size is allocated to hold the data, and the data is read from the FITS file. Upon output, the data in the buffer is converted to double precision. The positions of the gap columns (due to the presence of the beamsplitter used to direct solar light to the two SOLIS/VSM cameras) are also read from the appropriate FITS header keywords (`GAPCOL1` and `GAPCOL2`).

#### 4.3.2 Intensity Thresholding

While VFISV is meant to invert every single pixel in the field-of-view (FOV), some concessions must be made about what qualifies as truly invertible data. Before any inversion calculations are made for a particular pixel, the code determines whether it should actually attempt to do so, based on intensity considerations. The following list outlines the situations in which no inversion is attempted for a given pixel:

- **Sky pixels:** These are low-intensity pixels outside the image-plane solar disc. Intensity thresholds for ignoring these pixels are different for Rockwell and Sarnoff camera eras, and are set in the `SET_CAMTYPE_PROPERTIES()` routine, as outlined in Section 4.2.1.
- **Gap columns:** These are pixels (near the horizontal center of the FOV) containing non-invertible data resulting from the presence of the beamsplitter which directs solar light to camera A/B. `GAPCOL1` and `GAPCOL2` header keywords are read from the Level-0.5 FITS file,

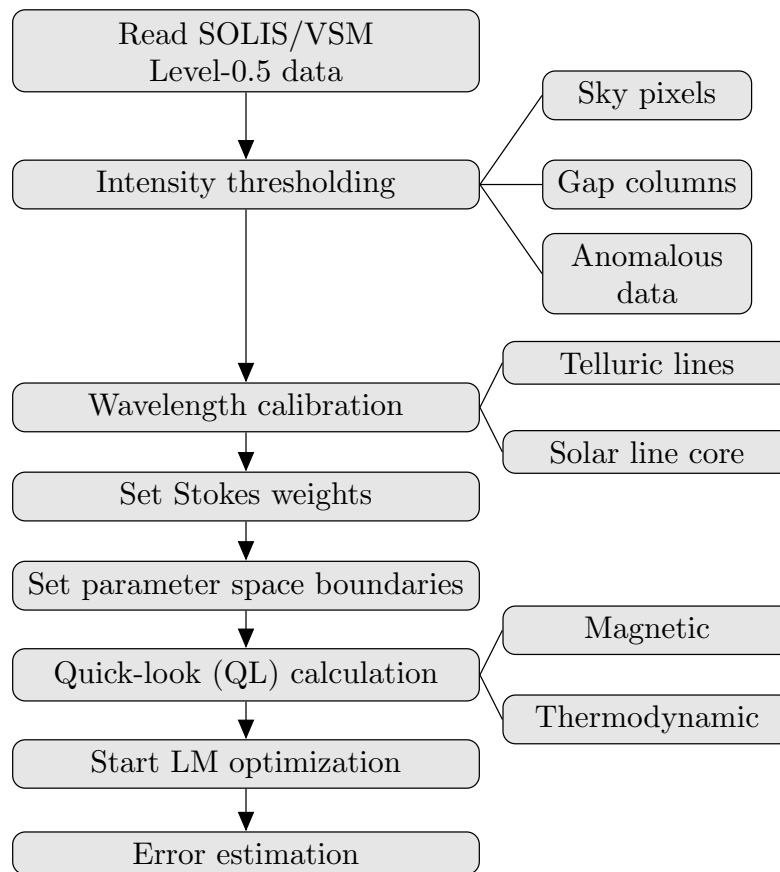


Figure 2: Schematic flowchart showing the major steps of the inversion subroutine, `INVERT_SCANLINE()`.



and denote the starting and ending indices, respectively, of this gap in the data. No thresholding based on intensity is performed in the gap, and the inversion code simply skips over pixels in the gap.

- **Anomalous data:** These pixels are likely the result of “garbage” at the extreme edges of the FOV; they may be straggler sky pixels, or the result of errors in the camera CCD readout, or something else. If (1) the maximum total polarization signal is equal to zero, and/or (2) the continuum intensity of the neighborhood-averaged non-magnetic Stokes  $I$  profile is zero, the inversion code simply skips over these pixels.

### 4.3.3 Wavelength Calibration

Once the spectra in a given pixel have been validated as containing invertible data, the next step is to calibrate the observed wavelength scale. This is done by taking advantage of the two nearby terrestrial absorption lines of molecular oxygen. They have a known wavelength separation, so that we can establish the spectral dispersion by finding their positions to subpixel accuracy. Locating the telluric line-core region (to the nearest pixel) is done with a quasi-dynamic watershed algorithm, in which a suitably large window surrounding each telluric line is searched in a “geographic” manner to find the minimum intensity. Consider the line profile as a topological surface; the watershed algorithm adds “droplets” at each wavelength point in the telluric window. Each droplet travels downhill (in the negative gradient direction) until it encounters a local minimum, where it stops. The wavelength point which has accumulated the most droplets is marked as the core of the telluric line. This has distinct advantages over a simple search for the minimum intensity of the line. Since the telluric lines do not shift due to solar rotation, using a large range of wavelengths when considering telluric line boundaries can “bleed” into the solar line. It is possible (and indeed happens) that there can be a wavelength point in the solar line at a lower intensity than the telluric line-core, which would falsely assign a solar line wavelength as the telluric line-core. The watershed skirts this issue by allowing *some* misidentifications without influencing the final identification. Some droplets may indeed fall into the solar line, but the majority of the droplets will find their way into the telluric line. This method is also insensitive to any global shifts in the spectrum which might cause the telluric line(s) to wander outside the (constant, hard-wired) telluric window. Should the identified line-core position fall outside the telluric window, the watershed algorithm recursively calls itself with a smaller telluric window until the identified minimum falls within that window. This method has proven to be extremely robust.

Once the telluric line-cores have been identified, the line-core regions are fit with a second degree polynomial to refine the line-core positions to sub-pixel accuracy. If the two telluric line-core positions (in fractional pixels) are denoted  $s_1$  and  $s_2$  respectively, then the spectral dispersion,  $\Delta\lambda_{\text{disp}}$ , is given by:

$$\Delta\lambda_{\text{disp}} = \frac{\Delta\lambda_{O_2}}{s_2 - s_1}, \quad (23)$$

where  $\Delta\lambda_{O_2}$  is the known telluric line separation. This quantity (in Å) is given in the file `params.f90` as `DLAMO2 = 0.76220703D0`. With a known spectral dispersion, and the position of one of the telluric lines known to be  $6302.0005\text{Å}$ , a calibrated wavelength offset scale can be obtained for each line. This wavelength offset scale is expressed as a shift from the line-core position of each line. The line-core positions for the solar lines are found by smoothing the wavelength derivative of Stokes  $I$  with a Gaussian kernel, then searching for the zero-crossing of the (smoothed) result.

Consistency is maintained by allowing the 6302.5Å line-core to vary a little around a 41-pixel offset from the core of the 6301.5 line. This helps prevent misidentifications due to (e.g.) highly split lines, or some anomalous data in the line profile. Centering the wavelength scale on the solar line-core means that positions on the line profile to the blue-side of the line-core have negative shifts, and red-side line profile positions have positive shifts. This transforms the reduced wavelength array ( $v$  in Equation (12)) used in the Voigt- and Faraday-Voigt profile synthesis to:

$$v = \frac{\lambda - \lambda_0(v_{\text{los}}/c) \pm \Delta\lambda_Z}{\Delta\lambda_D}. \quad (24)$$

Since this is done only once in the establishment of the wavelength shift array, it is much more efficient than using arrays of absolute wavelengths, and saves many repeated calculations in the `SYNTHESIS()` subroutine.

#### 4.3.4 Parameter Space Boundaries

The boundaries of the parameter space used in the inversion must be suitably large enough to capture the range of physical atmospheric conditions present in the solar photosphere, but restricted enough to allow the inversion to converge to a solution in a reasonable amount of time. The ME model parameters used in the inversion are subject to the general box constraints shown below. If any model parameter violates its upper/lower box constraints at any point during the inversion, it is reset to the corresponding upper/lower value.

$$[\min(B), \max(B)] = [0, 3500] \text{ G} \quad (25)$$

$$[\min(\gamma), \max(\gamma)] = [0, 180]^\circ \quad \star \quad (26)$$

$$[\min(\chi), \max(\chi)] = [0, 180]^\circ \quad (27)$$

$$[\min(v_{\text{los}}), \max(v_{\text{los}})] = [-7 \times 10^5, 7 \times 10^5] \text{ cm/sec} \quad \star \quad (28)$$

$$[\min(\Delta\lambda_D), \max(\Delta\lambda_D)] = [10, 65] \text{ mÅ} \quad (29)$$

$$[\min(a_{\text{dc}}), \max(a_{\text{dc}})] = [0, 5] \quad (30)$$

$$[\min(\eta_0), \max(\eta_0)] = [1, 100] \quad (31)$$

$$[\min(S_0), \max(S_0)] = [0, I_c] \quad \star \quad (32)$$

$$[\min(\mu S_1), \max(\mu S_1)] = [0, I_c] \quad (33)$$

$$[\min(\alpha), \max(\alpha)] = [0, 1] \quad (34)$$

$$[\min(v_{\text{mac}}), \max(v_{\text{mac}})] = [1 \times 10^{-5}, 5 \times 10^5] \quad (35)$$

Parameters marked by a  $\star$  above are dealt with a little more rigorously, as follows:

- Instead of using constant boundaries for the inclination angle,  $\gamma$ , which encompass both positive and negative polarities, the order of the Stokes  $V$  lobes is used to constrain the parameter space; if the positive Stokes  $V$  lobe is blueward of the negative Stokes  $V$  lobe, the inclination is positive, and constrained to  $[0, 90]^\circ$ . Conversely, if the negative lobe is blueward of the positive lobe, the inclination is thus constrained to  $[90, 180]^\circ$ . Quiet-sun pixels are liberally defined as those pixels whose quicklook magnetic filling factor,  $\alpha$  (see Section 4.3.5), is less than 0.025, and for these pixels the entire inclination range is used ( $\gamma \in [0, 180]^\circ$ ).

- Since we have already accurately determined the line-center wavelength, we limit the range of allowable LOS velocities to values such that the line is only allowed to be Doppler shifted by a maximum of  $\pm 1$  spectral pixel.
- As shown in Section 1, the source function parameters are constrained by  $S_0 + \mu S_1 = I_c$ . To satisfy this relation in the inversion, only the source function gradient,  $\mu S_1$ , is considered a free parameter of the fit (since it affects the amplitudes of the Stokes profiles), and  $S_0$  is then always calculated from the constraint relation.

#### 4.3.5 Quicklook (QL) Calculation(s)

The quicklook (QL) algorithm produces both a unique data product as well as an initialization for the ME inversion. It estimates the field strength, inclination, azimuthal angle, and magnetic filling-factor directly from the Stokes profiles, integrated over suitable wavelength ranges. The method is based on the technique in Ronan et al. (1987), whereby Taylor expansions of the relationship between intensity and circular/linear polarization profiles (for a normal Zeeman triplet) are utilized to calculate the longitudinal/transverse components of the magnetic field. Let us define the integrated Stokes profiles as:

$$\langle I \rangle = \int_{\lambda_L}^{\lambda_U} I_\lambda d\lambda \quad (36)$$

$$\langle Q \rangle = \int_{-\infty}^{\lambda_L} Q_\lambda d\lambda - 3.5 \int_{\lambda_L}^{\lambda_U} Q_\lambda d\lambda + \int_{\lambda_U}^{-\infty} Q_\lambda d\lambda \quad (37)$$

$$\langle U \rangle = \int_{-\infty}^{\lambda_L} U_\lambda d\lambda - 3.5 \int_{\lambda_L}^{\lambda_U} U_\lambda d\lambda + \int_{\lambda_U}^{-\infty} U_\lambda d\lambda \quad (38)$$

$$\langle V \rangle = \int_{-\infty}^{\lambda_0} V_\lambda d\lambda - \int_{\lambda_0}^{\infty} V_\lambda d\lambda, \quad (39)$$

where  $\lambda_0$  is the line-center wavelength. The quantity  $\lambda_{UL} = \lambda_0 \pm 1.5\Delta\lambda_{\text{FWHM}}$ , where  $\Delta\lambda_{\text{FWHM}}$  is the full width at half-maximum of the quiet-Sun Stokes  $I$  profile. Although some of the upper/lower limits above are  $\pm\infty$ , in practice any limit which reaches the (unpolarized) continuum will give the same results.

With the above definitions, the LOS and transverse (TRN) components of the magnetic field are given by:

$$B_{\text{LOS}} = C_{\text{LOS}} \left[ \frac{\langle V \rangle}{\langle I \rangle} \right] \quad (40)$$

$$B_{\text{TRN}} = C_{\text{TRN}} \left[ \left( \frac{\langle Q \rangle}{\langle I \rangle} \right)^2 + \left( \frac{\langle U \rangle}{\langle I \rangle} \right)^2 \right]^{\frac{1}{4}}, \quad (41)$$

from which the QL inclination angle,  $\gamma$ , can be derived as:

$$\gamma = \tan^{-1} \left( \frac{B_{\text{TRN}}}{B_{\text{LOS}}} \right). \quad (42)$$

The QL transverse azimuthal angle,  $\chi$ , can be similarly calculated from:

$$\chi = \frac{\pi}{2} - \frac{1}{2} \tan^{-1} \left[ \frac{-\langle U \rangle}{\langle Q \rangle} \right] \quad (43)$$

The QL magnetic filling-factor,  $\alpha$ , is calculated as in Bommier et al. (2009):

$$\alpha = \frac{[V_{\lambda}^2]_{\text{max}} \tan^2 \gamma}{[Q_{\lambda}^2 + U_{\lambda}^2]_{\text{max}} (I_c - I_0)}, \quad (44)$$

where  $I_0$  is the line-core intensity. We choose not to consider the filling-factor as a free parameter of the fit, but instead hold it fixed at the QL value for the duration of the inversion. Given the well-known degeneracy between magnetic field strength and filling-factor when trying to invert for them simultaneously, as well as the fact that the filling-factor is really a kind of zeroth-order attempt to account for sub-pixel structure, we do not consider this too restrictive of an assumption, especially considering the quality of the results produced by the QL filling-factor calculation.

The proportionality constants  $C_{\text{LOS}}$  and  $C_{\text{TRN}}$  have been determined *a priori* by linear regression between the LOS and transverse components as determined from SDO/HMI observations on a test dataset and the corresponding quantities multiplying the proportionality constants in Equations (40) and (41). The SDO/HMI magnetograms were rebinned and smoothed using a Gaussian kernel to match the size and spatial sampling of SOLIS/VSM. This was accomplished by maximizing the cross-correlation between the SOLIS/VSM and SDO/HMI magnetograms as a function of (e.g.) smoothing kernel size. As implemented in the VFISV code, the proportionality constants were found to have the values:

$$C_{\text{LOS}} = 1.6833 \times 10^4 \quad (45)$$

$$C_{\text{TRN}} = 8.6960 \times 10^3 \quad (46)$$

It should be noted that these coefficients may need to be recalculated, particularly if any changes are made to the Lev0 code, if any hardware is swapped, or hardware settings changed, since these coefficients are derived from spectra with a given (e.g.) exposure time, frame rate, etc.

Thermodynamic model parameters are initialized in a less-rigorous way, simply to obtain decent starting values for the inversion; an approximate temperature is determined by referencing the continuum level to a nearby continuum wavelength in the atlas spectrum of Labs and Neckel (1968), and inverting the Planck function to solve for temperature. This reference intensity is  $3.11 \times 10^{14} \text{ ergs cm}^{-2} \text{ s}^{-1} \text{ sr}^{-1} \text{ cm}^{-1}$  at  $\lambda_{\text{ref}} = 6306.0 \text{ \AA}$ . From the temperature, we can then derive estimates of the Doppler width ( $\Delta\lambda_D$ ), damping parameter ( $a_{\text{dc}}$ ), and line-to-continuum opacity ratio ( $\eta_0$ ). The source function continuum,  $S_0$ , is initialized to zero, and its gradient,  $\mu S_1$ , is set to  $I_c$ , in accordance with the constraint on the sum of these two parameters. LOS velocity is also initialized to zero.

#### 4.3.6 Stokes Weights

The weights  $w_{ij}$  entering into Equation (21) are used to adjust the relative importance of deviations between the synthesized and observed Stokes profiles. Here, the  $j$  index is dropped from the

weights; they are taken as constant over the spectral line, but distinct for each of the four Stokes profiles. After *exhaustive* testing of various different weighting schemes, the following weights have been adopted, since they produce the best results in terms of synthetic fits to the observed line profiles while minimizing spurious pixel-to-pixel variations:

$$w_I = \frac{1}{I_c} \quad (47)$$

$$w_{QUV} = \left[ \mathbf{maxval} \left( \sqrt{Q_\lambda^2 + U_\lambda^2 + V_\lambda^2} \right) \right]^{-1}. \quad (48)$$

This has the effect of roughly equalizing the importance of deviations in Stokes  $I$ ,  $Q$ ,  $U$ , and  $V$  which contribute to the total  $\chi^2$  merit function value, provided there is adequate signal. For example, consider the situation of a sunspot umbral pixel at disc-center. In this case, Stokes  $V$  will have a strong signal due to the strong LOS field component, while Stokes  $Q$  and  $U$  will be dominated by noise. Therefore,  $w_{QUV}$  will be close to the maximum absolute value of the Stokes  $V$  profile. Along with the  $w_I$  weight, this will ensure that deviations in Stokes  $I$  and  $V$  contribute roughly equally to the  $\chi^2$  value. Conversely, since the Stokes  $V$  amplitude is much greater than that of Stokes  $Q$  and  $U$  (which are noise-dominated), application of these weights to Stokes  $Q$  and  $U$  will drastically reduce the importance of their contributions to the  $\chi^2$  value. Similar arguments can be made for any other combination of strong/weak Stokes  $Q$ ,  $U$ , and  $V$  profiles.

In addition, to further decrease the importance of Stokes  $Q$ ,  $U$ , and  $V$  profiles in the quiet-sun (which are noise-dominated), the Stokes  $Q$ ,  $U$ , and  $V$  weights are all multiplied by a simple function of the QL filling-factor,  $\alpha$ . This has the effect of retaining the original weights in strong field pixels while further decreasing the importance of Stokes  $Q$ ,  $U$ , and  $V$  in quiet-Sun pixels, where these signals are dominated by noise. It is well known that the presence of noise in these Stokes profiles can lead an inversion to falsely interpret some of that noise as real signal, which can in turn lead to artificially-high field strengths and poor profile fits. The modification of the Stokes weights by a function of the filling factor is an effective way to decrease the likelihood that noise-dominated Stokes profiles will contribute to the fit in a meaningful way. The functional form of this modification is:

$$f(\alpha) = \mathbf{min}(\alpha + 0.05, 1), \quad (49)$$

such that  $w_{QUV} \leftarrow f(\alpha)w_{QUV}$ . Note that  $f(\alpha)$  has a floor of 0.025 and a ceiling of 1. While in theory the floor should be 0 (to completely de-weight Stokes  $Q$ ,  $U$ , and/or  $V$  profiles which are solely noise), I have noticed that this case tends to produce sharp boundaries in the inverted parameters at the edge of magnetically active regions. Having a small but non-zero floor smoothes out these discontinuities satisfactorily.

#### 4.4 Stokes Profile Synthesis Module

The synthesis code for calculating Stokes profiles takes the vector ME model parameters and returns the Unno-Rachkovsky solutions to the PRTE. The elements of the propagation matrix,  $\mathbf{K}_\lambda$ , are evaluated and are used to calculate the Unno-Rachkovsky solutions,  $\mathbf{I}_\lambda^M$ , for both the 6301.5Å and 6302.5Å lines. These synthesized lines are superimposed to create the full synthetic line profile in the appropriate wavelength range. This full line profile is mixed with the non-magnetic component, according to the value of  $\alpha$ . We correct for scattered (or stray) light in the observations at the

5% level by adding the appropriate amount of scattered light to the synthesized profiles (as opposed to removing the scattered light from the observed spectra themselves before the inversion). For a scattered light fraction,  $s < 1$ , the standard correction has the form:

$$I_{\text{corr}} = \frac{I_{\text{obs}} - s\langle I_{\text{obs}} \rangle}{1 - s}, \quad (50)$$

where  $\langle I_{\text{obs}} \rangle$  denotes the average observed intensity in the line profile. We invert this expression to obtain a synthesized Stokes  $I$  profile that has had the proper amount of scattered light *added* to it:

$$I_{\text{syn}} = (1 - s)I_{\text{syn}} + s\langle I_{\text{syn}} \rangle. \quad (51)$$

The 6302.5Å line is a normal Zeeman triplet, with a single  $\sigma_r$ ,  $\sigma_b$ , and  $\pi$ -component; the 6301.5Å line is an anomalous Zeeman triplet with multiple Zeeman subcomponents. Each component depends non-linearly on the absorption ( $\phi_\lambda$ ) and anomalous dispersion ( $\psi_\lambda$ ) profiles, calculated from the Voigt and Faraday-Voigt lineshapes, respectively. The `VOIGT_RFA()` algorithm uses the rational function approximation (RFA) of Hui et al. (1978). Let

$$R(z) = \frac{A(z)}{B(z)}, \quad (52)$$

where  $A(z)$  and  $B(z)$  are complex polynomials of the complex number  $z = a_{\text{dc}} - vi$ . Then  $H(a_{\text{dc}}, v) = \text{Real}[R(z)]$  and  $F(a_{\text{dc}}, v) = \text{Sign}(v)\text{Imag}[R(z)]$ . This algorithm is very fast and accurate, and has been tested for accuracy against the built-in IDL function `VOIGT()`. Over the applicable domain of  $a_{\text{dc}}$  relevant for photospheric spectral line inversion ( $a_{\text{dc}} \sim 0.5$ ), the two methods differ by at most an average of a few times  $10^{-7}$  in absolute value, as seen in Figure 3. The maximum error is about an order of magnitude greater than the average error, but these larger errors occur far out in the continuum, where the computation has less effect on the line-shape. The complex polynomial coefficients for  $A(z)$  and  $B(z)$  used in the RFA are defined in `params.f90` in the `ACOEFF` and `BCOEFF` variables.

The synthesis module also calculates the derivatives of the synthesized Stokes profiles with respect to the model parameters,  $\partial \mathbf{I}_\lambda^M / \partial p_i$ . Under the ME assumptions, these derivatives can be evaluated analytically. To increase the speed of the synthesis, and to avoid unnecessary calculations, these derivatives are evaluated only if the  $\chi^2$  merit function value has improved, except when a reset is performed (see Section 4.4.1), in which case the derivatives *must* be updated immediately.

#### 4.4.1 Levenberg-Marquardt Considerations

The QL model parameters are used as a starting point for synthesizing Stokes profiles; these synthesized profiles are compared to the observed profiles, and the  $\chi^2$  goodness-of-fit metric is evaluated. The QL model parameters are then iteratively improved upon by a modified Levenberg-Marquardt (LM) algorithm, by generating model parameter perturbations, synthesizing new Stokes profiles, and judging whether the new profiles are an improvement over the old profiles. This proceeds until one or more termination criteria are met, at which point the model vector corresponds to the model parameters of the ME atmosphere in which the observed Stokes profiles were formed. This iterative LM inversion is skipped entirely when running in “preview mode”.

In order to make improvements to the fit between the observed and synthesized profiles, we need to be able to generate perturbations in the model parameters in a self-consistent way. This is done

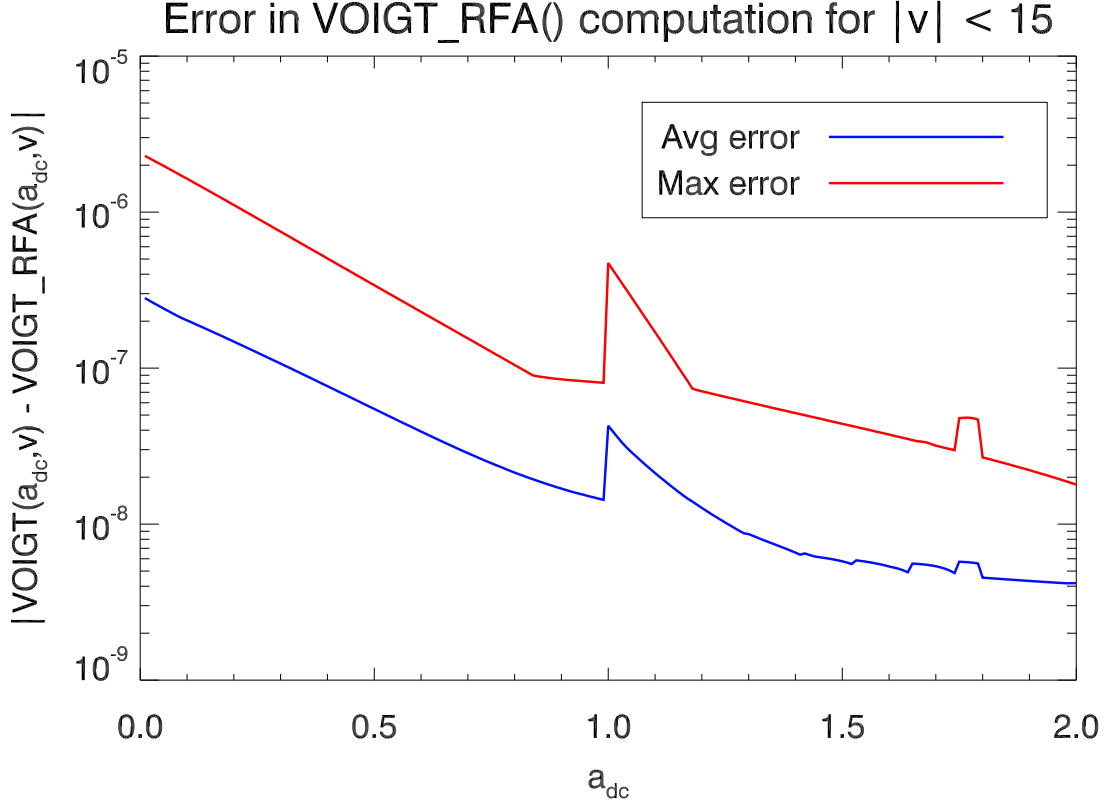


Figure 3: Absolute errors between `VOIGT_RFA()` and the IDL implementation.

by monitoring the curvature of the  $\chi^2$  hypersurface, through the gradient vector and Hessian matrix. Recalling Equation (21), we can calculate the gradient vector and Hessian matrix in a straightforward way. The gradient with respect to the model parameters is therefore given by

$$[\nabla\chi^2(\mathbf{p})]_i = \frac{\partial\chi^2(\mathbf{p})}{\partial p_i} = -\frac{2}{\nu} \sum_{k=IQUV} w_k^2 \sum_{N_\lambda} [\mathbf{I}_\lambda^{O_k} - \mathbf{I}_\lambda^{M_k}] \frac{\partial\mathbf{I}_\lambda^{M_k}}{\partial p_i}, \quad (53)$$

and the Hessian matrix of partial derivatives is given by

$$[\mathbf{H}(\mathbf{p})]_{ij} = \frac{\partial^2\chi^2(\mathbf{p})}{\partial p_i \partial p_j} = \frac{2}{\nu} \sum_{k=IQUV} w_k^2 \sum_{N_\lambda} \left[ \frac{\partial\mathbf{I}_\lambda^{M_k}}{\partial p_i} \frac{\partial\mathbf{I}_\lambda^{M_k}}{\partial p_j} - [\mathbf{I}_\lambda^{O_k} - \mathbf{I}_\lambda^{M_k}] \frac{\partial\mathbf{I}_\lambda^{M_k}}{\partial p_i \partial p_j} \right]. \quad (54)$$

It is conventional to disregard the second-derivative term in the above equation, since it may have a destabilizing effect in the early stages of the optimization, when the deviations between the model and observations are expected to be large. At later stages (i.e. after improvements to the fit), the contribution from this term will tend to cancel out when summed over wavelength, due to the presence of the  $\mathbf{I}_\lambda^{O_k} - \mathbf{I}_\lambda^{M_k}$  term. Therefore, the true Hessian matrix is approximated by the product of the corresponding first derivatives:

$$[\mathbf{H}(\mathbf{p})]_{ij} = \frac{\partial^2\chi^2(\mathbf{p})}{\partial p_i \partial p_j} \approx \frac{2}{\nu} \sum_{k=IQUV} w_k^2 \sum_{N_\lambda} \left[ \frac{\partial\mathbf{I}_\lambda^{M_k}}{\partial p_i} \frac{\partial\mathbf{I}_\lambda^{M_k}}{\partial p_j} \right] \quad (55)$$

Given the above equations describing the curvature of the  $\chi^2$  hypersurface, we can relate them to give a set of linear equations:

$$\mathbf{H}(\mathbf{p}) \cdot \Delta\mathbf{p} = \nabla\chi^2(\mathbf{p}), \quad (56)$$

which may be solved for the model perturbations,  $\Delta\mathbf{p}$ . Contributions from Stokes *I* to  $\chi^2(\mathbf{p})$ ,  $\nabla\chi^2(\mathbf{p})$ , and  $\mathbf{H}(\mathbf{p})$  for wavelengths within the telluric window are neglected, to prevent these deviations from contributing to the solution procedure. For stability and robustness, these linear equations are solved using the Singular Value Decomposition, as implemented in the `DGESVD` () routine from the LAPACK library.

The LM algorithm uses an adaptive “step-size” governor parameter,  $\lambda$ , to allow the algorithm to dynamically and smoothly switch itself between the quadratic approximation and gradient-descent paradigms, when solving for the model parameter perturbations in each iteration; the diagonal elements of the Hessian matrix are multiplied by the factor  $1 + \lambda$ , so that

$$[\mathbf{H}(\mathbf{p})]_{ii} = (1 + \lambda) [\mathbf{H}(\mathbf{p})]_{ii}. \quad (57)$$

For  $\lambda \ll 1$ , this modification has little effect, so that the solution to the above set of linear equations is roughly the quadratic approximation, in which the neighborhood of the current vector  $\mathbf{p}$  is approximated by a surface with quadratic curvature, and the model parameter perturbations calculated from Equation (56) allow  $\mathbf{p}$  to jump directly to the minimum of that surface. Conversely, for  $\lambda \gg 1$ , the Hessian matrix becomes diagonally-dominant, and this has the effect of approximating a gradient-descent algorithm when calculating the model parameter perturbations. The value of the  $\lambda$  parameter for the next iteration is adjusted according to the (non-)success of the current iteration:

$$\lambda_{n+1} = \begin{cases} \lambda_n/\epsilon_-, & \text{if } \chi_n^2 \leq \chi_{\text{best}}^2 \\ \epsilon_+ \lambda_n, & \text{if } \chi_n^2 > \chi_{\text{best}}^2 \end{cases} \quad (58)$$

where  $\epsilon_- = 5$  and  $\epsilon_+ = 3$ . Historically, many algorithms set  $\lambda_n$  to be increased and decreased by the same factor. The asymmetric adjustment used here is commonly known as “delayed gratification” and has been shown to have better performance characteristics than the symmetric update; many different  $\lambda$ -update strategies were tested during development, and this method did provide the best performance in terms of speed of convergence and solution quality. So, for a successful iteration in which an improvement in the  $\chi^2$  goodness-of-fit metric is found, the model vector lies closer to the minimum of the  $\chi^2$  hypersurface (i.e. closer to the region where the quadratic approximation holds). Therefore, we decrease the  $\lambda$  factor, making the algorithm behave more like it is calculating an exact solution for the minimum. To prevent  $\lambda$  from getting too small and wasting computational effort, we set a minimum value,  $\lambda_{\text{min}} = 10^{-4}$ . For a non-successful iteration in which no improvement is found, the  $\lambda$  factor is increased and the algorithm attempts to traverse the parameter space by taking ever-smaller steps in the negative gradient direction to improve the fit. This procedure is iterated until one or more convergence metrics are satisfied (more on this in Section 4.4.2). A flowchart of the LM optimization procedure is shown in Figure 4.

Two “insurance policy” strategies are employed within the LM inversion algorithm, to ensure that it does indeed converge to a good solution in the face of an unforeseen anomalous runtime condition: a recovery strategy and a reset strategy. The details of these strategies are provided below.



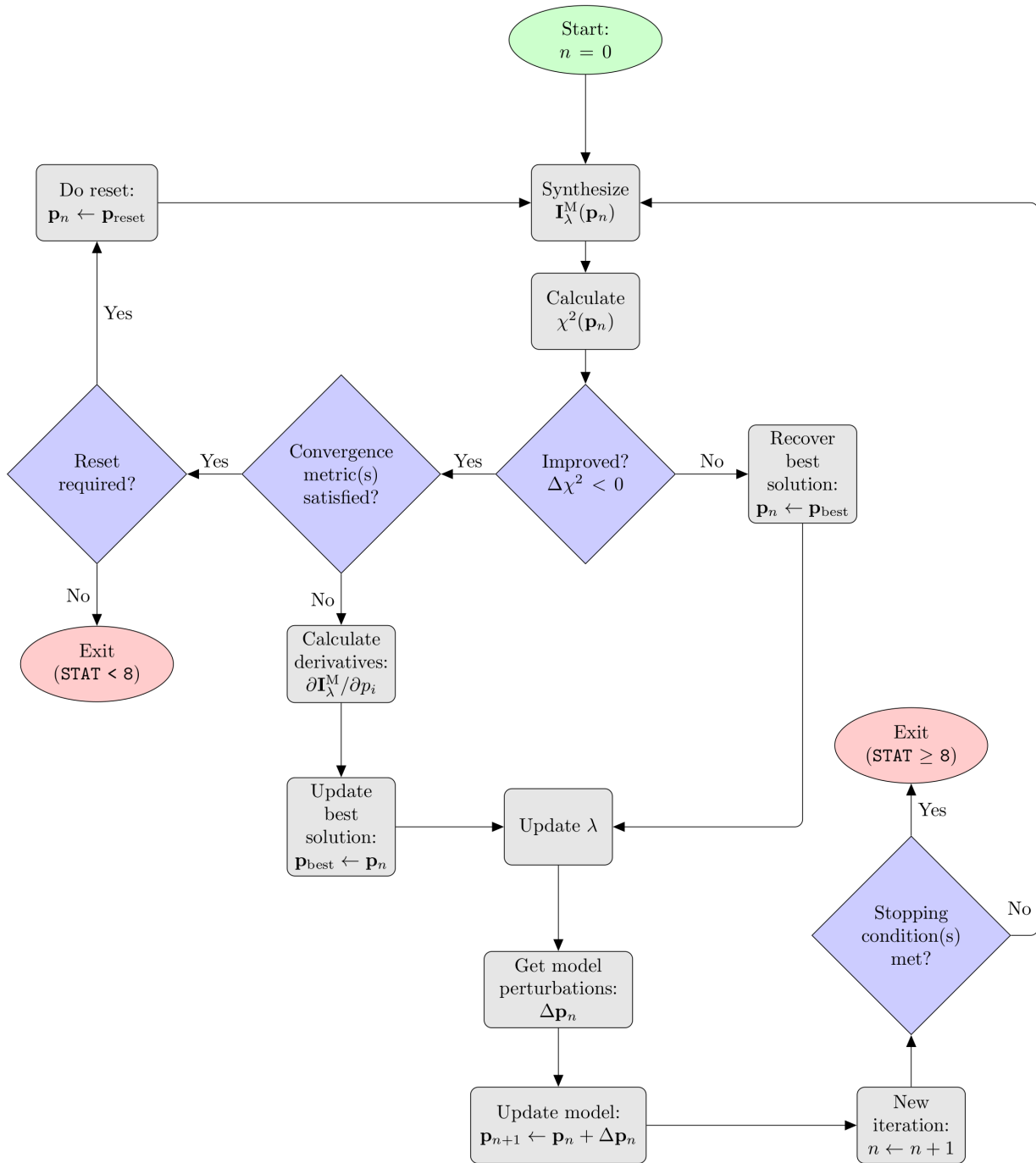


Figure 4: Schematic flowchart detailing the operation of the LM optimization.

- **RECOVERY STRATEGY:** Should something go wrong at any point in the inversion (e.g. a NaN or Inf crops up), for whatever reason, a fallback mechanism is in place to re-establish a good point/direction in parameter space. The downhill simplex method of Nelder and Mead (1965), commonly known as the “amoeba” algorithm, is used. The last known good solution (before the NaN/Inf showed up, e.g.) is used to randomly spawn a non-degenerate simplex, which then attempts to move in the negative gradient direction on the  $\chi^2$  parameter space by “reflecting” the highest vertex of the simplex through the opposite face of the simplex to a lower point. Expansions and contractions of the vertex can also be performed, to take larger or smaller steps, respectively. This continues until all vertices of the simplex have converged on each other to within some specified tolerance (defined in `params.f90` as `AMOEBA_FTOL`). The best vertex then overwrites the last known good solution, and the LM algorithm proceeds as normal. To avoid too much time being spent in this recovery phase, the convergence tolerance for the amoeba algorithm is much larger than the normal  $\chi^2$  convergence tolerance (see next Section), and a relatively small maximum number of amoeba iterations is used. The SOLIS/VSM remix of the VFISV code is very stable and robust, so in practice this recovery strategy is *very* rarely employed. But, it never hurts to be prepared.
- **RESET STRATEGY:** Occasionally, some pixels do not find an adequate solution (i.e.  $\chi^2$  does not improve “enough” over the initial estimate). When this occurs, the model vector is re-initialized using the best-fit model from the previous pixel (along the scanline), various bookkeeping variables are re-initialized, and the inversion starts over with the new model vector. In the case where multiple resets are required, the re-initialized model vector is perturbed randomly (the scale of the perturbations becomes proportionately larger for repeated resets). This strategy ensures that any spurious pixel-to-pixel variation in the magnetograms (due to non-convergence of the solution trajectory) is minimized. As an insurance policy to guard against a potential infinite loop, the maximum number of allowed resets is set in `params.f90` as `MAX_RESETS=5`.

#### 4.4.2 Convergence Strategies/Criteria

The following conditions are used to signal successful convergence of the inversion algorithm, and the value of `CONVERGENCE_FLAG` is set to indicate which convergence criterion was met. To signal successful convergence, we require any combination of the following conditions to be met for two (2) consecutive successful iterations:

- **CONVERGENCE CRITERIA 1:** An improvement produces a change in  $\chi^2$  less than a specified convergence tolerance (`FCONV_TOL`), defined in `params.f90`. In this case, `CONVERGENCE_FLAG = 1` if no reset was triggered. If a reset was triggered during the inversion, `CONVERGENCE_FLAG = 5`.
- **CONVERGENCE CRITERIA 2:** An improvement produces a change in each model parameter (relative to the current best model) that is less than a specified convergence tolerance (`XCONV_TOL`), defined in `params.f90`. In this case, `CONVERGENCE_FLAG = 2` if no reset was triggered. If a reset was triggered during the inversion, `CONVERGENCE_FLAG = 6`.
- **CONVERGENCE CRITERIA 3:** The LM  $\lambda$  parameter exceeds a maximum value (`LAMBDA_MAX`), defined in `params.f90`. This large  $\lambda$  value indicates that the algorithm has spent many iterations in the “gradient descent” paradigm of the solution procedure, and therefore is likely in a low-curvature region of the parameter space, i.e. near a minimum in the parameter space.

The current implementation sets `LAMBDA_MAX=1E+4_DP`. In this case, `CONVERGENCE_FLAG = 3`. If a reset was triggered during the inversion, `CONVERGENCE_FLAG = 7`.

In addition to the convergence criteria above, we must employ some stopping criteria to terminate the inversion if the solution fails to converge in a timely fashion. The two stopping criteria employed are as follows:

- **STOPPING CRITERIA 1:** If the inversion has not signalled convergence after `MAX_ITER`s iterations (defined in `params.f90`, default 200), the inversion stops iterating and reports the best solution it found. In this case, we cannot assume the best-found model parameters are indeed the best-fit model parameters, and so any uncertainty calculation may not be meaningful. If no reset was triggered during the inversion, `CONVERGENCE_FLAG = 4`. If a reset was triggered, `CONVERGENCE_FLAG = 8`.
- **STOPPING CRITERIA 2:** If too many resets are triggered during the inversion, this is likely a pixel with Stokes data of anomalous or strange morphology, and it is likely the inversion may not ever find a good solution. The maximum number of allowable resets for a single pixel is specified by the `MAX_RESETS` parameter (defined in `params.f90`, default 5). If a pixel inversion fails due to too many resets, `CONVERGENCE_FLAG = 9`.

#### 4.4.3 Error Estimation

Once the LM algorithm has converged, we can obtain estimates of the standard errors/uncertainties in the fitted model parameters. To do this, the inverse of the Hessian matrix, known as the covariance matrix, must be calculated. This matrix describes the covariances between pairs of the fitted model parameters,  $\mathbf{p}_{\text{best}}$ . The standard variances in the model parameters are proportional to the diagonal elements of the covariance matrix, and are given by:

$$\sigma_i^2 = \frac{\chi^2(\mathbf{p}_{\text{best}})}{N_\lambda} [\mathbf{H}^{-1}(\mathbf{p}_{\text{best}})]_{ii} . \quad (59)$$

However, this standard definition relies on the assumption that, on exit, the gradient of  $\chi^2$  is equal to zero, and any uncertainties in the fit are due to noise in the observed spectra. The LM algorithm typically does not reach a zero-gradient solution (in a mathematical sense), so that these error estimates systematically underestimate the true errors. This is because the uncertainty in the fit may not be due solely to noise, but rather to the distance between the true minimum and the returned  $\mathbf{p}_{\text{best}}$  which has a value of  $\chi^2(\mathbf{p}_{\text{best}})$ . Sanchez Almeida (1997) instead developed an error estimate which does not depend on the above assumptions, so is safe to evaluate the uncertainties in the model parameters on exit. It provides a range of free parameters whose synthetic Stokes profiles deviate from the observed Stokes profiles by an amount equal to  $\chi^2(\mathbf{p}_{\text{best}})$ , thus providing a statistically significant estimate of the uncertainty. This new estimate turns out to be

$$\sigma_i^2 = \frac{\chi^2(\mathbf{p}_{\text{best}})}{N_{\text{free}}} [\mathbf{H}^{-1}(\mathbf{p}_{\text{best}})]_{ii} , \quad (60)$$

where  $N_{\text{free}}$  is the number of free parameters of the fit. Note that, since  $N_{\text{free}} \ll N_\lambda$ , we are now no longer underestimating the errors. These standard errors are only accurate provided the final best model parameters are indeed close to the minimum of the  $\chi^2$  hypersurface. For cases where convergence to the minimum of the parameter space cannot be assumed (i.e. when the maximum number of iterations were performed without signalling any convergence criteria), these errors are not likely to be very meaningful.

## 5 Output Format

VFISV writes separate standard SOLIS/VSM 6302v Level-1 data product FITS files containing both the QL and ME output of the code. However, when running in “preview mode”, only the Level-1 QL is actually written to a file. Regardless of the values of `SCAN_START`, `SCAN_END`, `PIX_START`, and/or `PIX_END` specified on the command line, these FITS files are sized to  $2048 \times 2048$  spatial pixels. The FITS files are staged in temporary directories, to be modified by later pipeline routines before being deployed to the keep. The Level-1 ME(QL) file contains 12(6) planes, and for completeness these planes are listed here in the order in which they appear in the output file. Each item is prefaced by an indication of which Level-1 data product it appears in (ME and/or QL).

- [ME/QL] Field Strength,  $B$  [Gauss] : Total magnetic field strength.
- [ME/QL] Azimuth,  $\chi$  [degrees] : Azimuthal angle of the transverse component (perpendicular to the LOS) of the vector magnetic field. The azimuth has not yet been disambiguated at Level-1, so lies in the range  $[-90,+90]^\circ$ . The zero-direction points horizontally to the right, in the image plane.
- [ME/QL] Inclination,  $\gamma$  [degrees] : The inclination of the magnetic field vector relative to the LOS. Inclination lies in the range  $[0,180]^\circ$ . Quiet-sun values may tend to  $90^\circ$  because of noise in the polarization profiles (which have different sensitivity to the magnetic field) being misinterpreted as signal. This does *not* mean the quiet-Sun fields are truly horizontal!
- [ME/QL] Continuum Intensity,  $I_c$  [counts] : The continuum intensity, calculated as the average Stokes  $I$  signal in the continuum window.
- [ME/QL] Magnetic Filling-Factor,  $\alpha$  [N/A] : The magnetic filling factor, defined as the fraction of the spatial pixel occupied by magnetic field. The filling factor lies in the range  $[0,1]$ . This parameter is not inverted, but held fixed at the QL value for the duration of the inversion.
- [ME] Doppler Width,  $\Delta\lambda_D$  [mÅ] : The Doppler width of the line.
- [ME] Line-to-Continuum Opacity Ratio,  $\eta_0$  [N/A] : The ratio of absorption coefficient in the line to that of the continuum.
- [ME] Standard Error in Azimuth,  $\sigma_\chi$  [degrees] : The standard uncertainty in the value of the azimuthal angle,  $\chi$ .
- [ME] Standard Error in Doppler Width,  $\sigma_{\Delta\lambda_D}$  [mÅ] : The standard uncertainty in the value of the Doppler width,  $\Delta\lambda_D$ .
- [ME/QL] Degree of Polarization,  $d_{\text{pol}}$  [N/A] : The degree of polarization, defined as

$$d_{\text{pol}} = \frac{\sqrt{\max(Q_\lambda^2) + \max(U_\lambda^2) + \max(V_\lambda^2)}}{I_c}. \quad (61)$$

- [ME] Damping Parameter,  $a_{\text{dc}}$  [units of  $\Delta\lambda_D$ ] : The atomic damping parameter of the line.
- [ME] Final  $\chi^2$  Value,  $\chi_{\text{min}}^2$  [N/A] : The final returned value of the  $\chi^2$  goodness-of-fit metric.

VFISV writes the output ME and QL FITS files with only a minimum FITS header. The SOLIS/VSM 6302v pipeline later overwrites this with a more detailed header containing standard required FITS header keywords, instrumental information from the observation metadata, and processing version information. An example of this SOLIS/VSM Level-1 standard header is shown below, for the observation taken on 08 July 2015 (k4v9s150708t175025\_oid114363777241750\_cleaned) which resulted in the Level-1 file k4v91150708t175025.fts.

```

SIMPLE = T / file does conform to FITS standard
BITPIX = -32 / number of bits per data pixel
NAXIS = 3 / number of data axes
NAXIS1 = 2048 / length of data axis 1
NAXIS2 = 2048 / length of data axis 2
NAXIS3 = 12 / length of data axis 3
EXTEND = T / FITS dataset may contain extensions
METAKEY0= '----- Standard Keywords -----'
DATE-OBS= '2015-07-08T17:50:25' / Observation date & start time (UTC)
DATE = '2015-07-08T18:40:27' / file creation date (YYYY-MM-DDThh:mm:ss UT)
TELESCOP= 'solis ' / Telescope
INSTRUME= 'vsm ' / SOLIS instrument
OBSERVER= 'Detrick B.' / Observer name
OBS-SITE= 'NSO/Tucson' / Observation location
OBS-MODE= '6302v ' / Observation mode
OBS-TYPE= 'full-scan' / Observation type (dark, flat, full-scan)
STARTIME= 1436377825 / Obs-start in seconds since Jan. 1, 1970
STOPTIME= 1436379136 / Obs-stop in seconds since Jan. 1, 1970
QUALEND = 0 / Completeness: 0- complete, 1- partial obs.
QUALSEE = 0 / Seeing: 0- unknown, 1- bad, 5- excellent
QUALOBS = 0 / Obs quality: 0- nominal, 1- generic bad
QUALCHK = 0 / Qual-check method: 0- automatic
QMAXLEV = 3 / Maximum processing level: Level-3 (Nominal)
IMGUNT01= '(Mx/cm^2)' / Image units
IMGYP01= 'Field Strength' / Image type description
IMGUNT02= 'degrees ' / Image units
IMGYP02= 'Azimuth ' / Image type description
IMGUNT03= 'degrees ' / Image units
IMGYP03= 'Inclination' / Image type description
IMGUNT04= 'Counts ' / Image units
IMGYP04= '630 nm Continuum Intensity' / Image type description
IMGUNT05= 'N/A ' / Image units
IMGYP05= 'Fill Factor' / Image type description
IMGUNT06= 'milliAngstroms' / Image units
IMGYP06= 'Doppler Width' / Image type description
IMGUNT07= 'N/A ' / Image units
IMGYP07= 'Line to cont opacity ratio' / Image type description
IMGUNT08= 'deg ' / Image units
IMGYP08= 'Std-error (Azimuth)' / Image type description
IMGUNT09= 'milliAngstroms' / Image units
IMGYP09= 'Std-error (dopw)' / Image type description
IMGUNT10= 'N/A ' / Image units

```

```

IMGTYP10= 'Percent Polarization' / Image type description
IMGUNT11= 'N/A          ' / Image units
IMGTYP11= 'Damping parameter' / Image type description
IMGTYP12= 'Chi-square' / Image type description
IMGUNT12= 'N/A          ' / Image units
PUBLISH = 1 / Publish flag
METAKEY2= '----- Instrument Keywords -----'
OBS-ID = 'oid114363777241750' / SOLIS obs ID
ENDSTATE= 'NOMINAL ' / Last DHS state
CAMTYPE = 'sarnoff ' / CCD camera type
NFRAMES = 192 / Total number of frames per scanline
NSCANS = 2048 / Number of scanlines of observation
SCANINIT= 0 / Initial scanline offset
BITSHIFT= 2 / DAS Bit offset
GAPCOL1 = 951 / First column within gap (one-indexed)
GAPCOL2 = 1033 / Last column within gap (one-indexed)
M1-STAT = 1 / Window cover position
M2-STAT = 15450 / M2 focus position
M3-STAT = 45759 / Calibration position
M6-STAT = -13523 / Modulator position
M7-STAT = -3740 / Littrow lens position
M9-STAT = 10247 / Beam-splitter position
GR-TILT = 6266 / Grating tilt position
FOCALMSK= 0 / Focal plane mask: out(0) or in(1)
WAVELNTH= 630.2 / Observed wavelength (nm)
METAKEY3= '----- Data Provenance -----'
PROVERO = 13.1001 / Level-0 processing pipeline version
DDARKVER= 4.0831 / Dark-change cal-image version
VECTCAL = 'veccal_20150630.fts' / vector calibration used
DARK-ID = 'oid1143637774301744' / Dark obsid
FLAT-ID = 'oid1143637775501746' / Flat obsid
CHECKSUM= 'jGAjjE4jjE9jjE9j' / HDU checksum updated 2015-07-08T18:40:28
DATASUM = '2662345718' / data unit checksum updated 2015-07-08T18:40:28
END

```

## References

- Bommier, V., M. Martínez González, M. Bianda, H. Frisch, A. Asensio Ramos, B. Gelly, and E. Landi Degl'Innocenti (2009), "The quiet Sun magnetic field observed with ZIMPOL on THEMIS. I. The probability density function." *Astronomy & Astrophysics*, 506, 1415–1428.
- Hui, A.K., B.H. Armstrong, and A.A. Wray (1978), "Rapid computation of the voigt and complex error functions." *Journal of Quantitative Spectroscopy and Radiative Transfer*, 19, 509 – 516.
- Labs, D. and H. Neckel (1968), "The Radiation of the Solar Photosphere from 2000 Å to 100 μm." *Zeitschrift für Astrophysik*, 69, 1.
- Landi Degl'Innocenti, E. and M. Landolfi, eds. (2004), *Polarization in Spectral Lines*, volume 307 of *Astrophysics and Space Science Library*.

- Nelder, J. A. and R. Mead (1965), "A simplex method for function minimization." *Computer Journal*, 7, 308–313.
- Rachkovsky, D. N. (1962), "Magnetic rotation effects in spectral lines." *Izvestiya Ordena Trudovogo Krasnogo Znameni Krymskoj Astrofizicheskoj Observatorii*, 28, 259–270.
- Rachkovsky, D. N. (1963), "The theory of the absorption lines formation in a magnetic field. The case of a complete redistribution of quanta over the line frequencies." *Izvestiya Ordena Trudovogo Krasnogo Znameni Krymskoj Astrofizicheskoj Observatorii*, 30, 267–272.
- Rachkovsky, D. N. (1967), "The reduction for anomalous dispersion in the theory of absorption line formation in a magnetic field." *Izvestiya Ordena Trudovogo Krasnogo Znameni Krymskoj Astrofizicheskoj Observatorii*, 37, 56–61.
- Ronan, R. S., D. L. Mickey, and F. Q. Orrall (1987), "The derivation of vector magnetic fields from Stokes profiles - Integral versus least squares fitting techniques." *Solar Physics*, 113, 353–359.
- Sanchez Almeida, J. (1997), "Physical Properties of the Solar Magnetic Photosphere under the MISMA Hypothesis. I. Description of the Inversion Procedure." *The Astrophysical Journal*, 491, 993.
- Unno, W. (1956), "Line Formation of a Normal Zeeman Triplet." *Publications of the Astronomical Society of Japan*, 8, 108.